η	Tracking			PID		ECal		HCal	
	Momentum Resolution	Vertex Resolution	Min pT	Momentum Range	Separation	Energy Resolution	Min Energy	Energy Resolution	Min Energy
$-3.5 < \eta < -3.0$	$0.1\% \times \mathrm{P} \oplus 0.5\%$	N/A	100 MeV/c	≤ 7 GeV/c	3σ	$2\%/\sqrt{E} \oplus 1-3\%$	200 MeV/c^2	$50\%/\sqrt{E} \oplus 10\%$	$400-500$ MeV/c^2
$-3.0 < \eta < -2.5$	"	$30/\mathrm{p_T} \oplus 40\ \mu m$	"	"	"	"	"	"	"
$-2.5 < \eta < -2.0$	"	$30/\mathrm{p_T} \oplus 20\ \mu m$	"	"	"	"	"	"	"
$-2.0 < \eta < -1.5$	$0.05\% \times \mathrm{P} \oplus 0.5\%$	"	"	"	"	$7\%/\sqrt{E} \oplus 1-3\%$	"	"	"
$-1.5 < \eta < -1.0$	"	"	"	"	"	"	"	"	"
$-1.0 < \eta < -0.5$	"	$20/\mathrm{p_T} \oplus 5\ \mu m$	"	≤ 10 GeV/c	"	$10-12\%/\sqrt{E} \oplus 1-3\%$	"	$85\%/\sqrt{E} \oplus 10\%$	"
$-0.5 < \eta < 0.0$	"	"	"	"	"	"	"	"	"
$0.0 < \eta < 0.5$	"	"	"	"	"	"	"	"	"
$0.5 < \eta < 1.0$	"	"	"	≤ 15 GeV/c	"	"	"	"	"
$1.0 < \eta < 1.5$	$0.05\% \times \mathrm{P} \oplus 1.0\%$	$30/\mathrm{p_T} \oplus 20\ \mu m$	"	≤ 30 GeV/c	"	"	"	$50\%/\sqrt{E} \oplus 10\%$	"
$1.5 < \eta < 2.0$	"	"	"	≤ 50 GeV/c	"	"	"	"	"
$2.0 < \eta < 2.5$	"	"	"	"	"	"	"	"	"
$2.5 < \eta < 3.0$	$0.1\% \times \mathrm{P} \oplus 2.0\%$	$30/\mathrm{p_T} \oplus 40\ \mu m$	"	≤ 30 GeV/c	"	"	"	"	"
$3.0 < \eta < 3.5$	"	$30/\mathrm{p_T} \oplus 60\ \mu m$	"	≤ 20 GeV/c	"	"	"	"	"

Table 8.7: Summary of requirements

8.4 Exclusive Measurements

8.4.1 Deeply virtual Compton scattering and exclusive production of π^0 in ep

Deeply virtual Compton scattering (DVCS) and the hard exclusive production exclusive deeply of π^0 mesons off a nucleon play a prominent role in the studies of GPDs. DVCS gives access to chiral-even GPDs, which are important for the extraction of information on both the nucleon tomography and the energy-momentum tensor (EMT), including access to the total angular momentum of partons, as discussed in Sec. 7.2.2.

Hard exclusive production of π^0 mesons, on the other hand, gives access to chiral-odd GPDs, some of which are related to transversity distributions, which are extensively studied in SIDIS and Drell-Yan processes.

The similarity between the final states of DVCS and hard exclusive production of π^0, see Sec. 7.2.2, suggests that the detectability of both processes in an apparatus equipped with electromagnetic calorimeters (ECALs) can be studied together. Another reason for a joined study of this type is that DVMP π^0 may become a background to DVCS. This happens when one low-energy photon coming from π^0 decay misses ECALs, its energy is too low for a detection, or if two electromagnetic cascades induced by photons can not be distinguished from each other. A common analysis of DVCS and DVMP π^0 therefore allows to stress three main aspects of ECALs design: geometrical acceptance, energy thresholds and granularity.

The study presented in this subsection is based on two Monte Carlo generators. The first one is MILOU 3D, a recently updated version of MILOU [919], used to generate DVCS events. The original version of MILOU is supplied with two-dimensional (x_{Bj}, Q^2) lookup tables of DVCS sub-amplitudes, refereed to as Compton form factors (CFFs), while t-dependance of those factors is factorised out and modelled with either exponential or dipole Ansatz. This way of modeling of CFFs has been modified for the purpose of this study. Namely, MILOU 3D can now be supplied with three-dimensional $(x_{\mathrm{Bj}}, Q^2, t)$ tables, allowing one to take into account an interplay between all three variables, which is

important to describe data at energies lower than those available at HERA [920]. This modification allowed us to use two realistic GPD models to generate the lookup tables: KM [921–924] implemented in GeParD and GK [925–927] implemented in PARTONS [928]. These two models significantly differ by the construction, i.e. they are based on different schemes of GPD modelling, and they are constrained by different experimental data. The second generator is toyMC, which was developed for the purpose of this study. It assigns a weight to each generated event, which corresponds to either DVCS or DVMP π^0 cross-section. For this generator the lookup tables of cross-sections were generated with GK model, which includes chiral-odd GPDs crucial for the description of exclusive π^0 production. The amplitudes for DVMP π^0 were evaluated using GK formalism [925], which is based on the modified perturbative approach [929], allowing one to overcome the problem of infrared divergences that appear for transversely polarised virtual photons. Among many available versions of chiral-odd GK GPDs we have chosen the one that successfully describes cross-sections measured by COMPASS [930]. The kinematic domain covered by this measurement significantly overlaps that of EIC, particularly at its lowest beam energy configuration: 5 GeV $\times$ 41 GeV. Both generators can be interfaced with eic-smearer.

Figure 8.34, realized simulating 500k events with MILOU 3D, compares the DVCS kinematics generated according to KM20 [924] (blue) and GK [927] (red) for the lowest and highest beam energy configurations. The following cuts have been applied at generation level: $Q^2 > 1$ GeV^2, $0.01 < y < 0.95$, and $0.01 < |t|$ GeV^2 < 1.6. Both models predict a significant drop of the cross section with Q^2.The different $|t|$ distributions for GK (exponential) and KM20 (dipole) are also evident.

Using the same sample of generated DVCS events, we have also simulated the energy and pseudo-rapidity distributions of scattered electron and produced real photon in a DVCS process. Figure 8.35 visualizes these spectra for the lowest and highest beam energy configuration. At lower energies the electron is predicted to be scattered within the nominal combined EMCAL+Tracker acceptance of $|\eta| < 3.5$. At the top electron-beam energy, the peak in the scattered electron distribution is predicted to be at $\eta \ -3.6$. This is expected to be valid for other exclusive processes, making a slightly extended acceptance at backwards pseudo-rapidities beneficial for detection efficiency. Both models predict that the nominal $|\eta| < 3.5$ acceptance should be enough for detecting most of the produced photons, with a nearly perfect situation at smaller beam energies and a slight loss in efficiency at top beam energy, notably at very low values of x_B.

In order to asses the significance of π^0 background, the pseudo-rapidity distribution of photons from DVCS and exclusive π^0 production before applying the smearing is compared in Fig. 8.36. These histograms represent the sample of events generated with toyMC for the four beam energy configurations considered in this report and assume an integrated luminosity of $\mathcal{L} = 10$ fb^{-1} per each configuration. Two cuts were applied to the sample before making the histograms: $Q^2 > 1$ GeV^2 and $0.01 < y < 0.95$. The validity of y-cut was checked with a sample of events after applying the smearing. This study shows that at $y = 0.01$ one may expect the resolution of this variable at the order of $dy/y \approx 0.5$ for 5 GeV $\times$ 41 GeV and $dy/y \approx 1$ for 18 GeV $\times$ 275 GeV beam energy configuration. We conclude that for 18 GeV $\times$ 275 GeV and the assumed acceptance of $|\eta| < 3.5$ for both

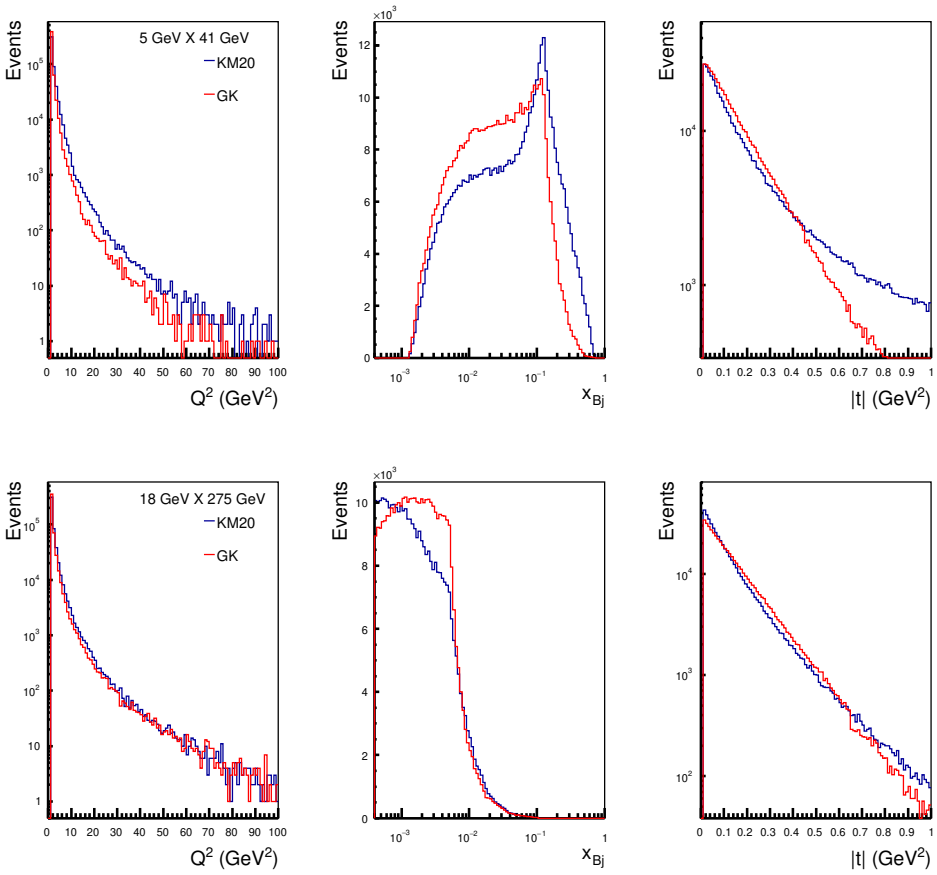

Figure 8.34: Kinematic distributions of DVCS events generated according to KM20 (blue) and GK (red) models.

electrons and photons one may expect to loose 14%/17% of DVCS events and 11%/12% of exclusive π^0 events, where the first number is due to the acceptance on electrons, while the second one is due to the acceptance on both electrons and photons. The loss is mainly seen for $Q^2 \approx 1$ GeV^2 events. The loss of DVCS events can be almost entirely recovered by slightly extending coverage in backwards pseudo-rapidity to $\eta < -3.7$ from the currently assumed value of $\eta < -3.5$. For lower beam energies the loos is smaller, in particular for 5 GeV $\times$ 41 GeV it is at the order of 1%.

The contamination of DVCS sample by misinterpreted exclusive π^0 events is demonstrated with Fig. 8.37, where the ratio of events in bins of (x_{Bj}, Q^2) is shown for 5 GeV $\times$ 41 GeV beam energies. This energy configuration is chosen because of the relative event yield (cf. Fig. 8.36) being the largest one compering to other configurations. The plot is made for the sample of events generated with toyMC after applying $Q^2 > 1$ GeV^2 and $0.01 < y < 0.95$ cuts, requiring both electrons and photons to be reconstructed assuming $|\eta| < 3.5$ acceptance. With no additional cuts on energy thresholds for the detection of photons in

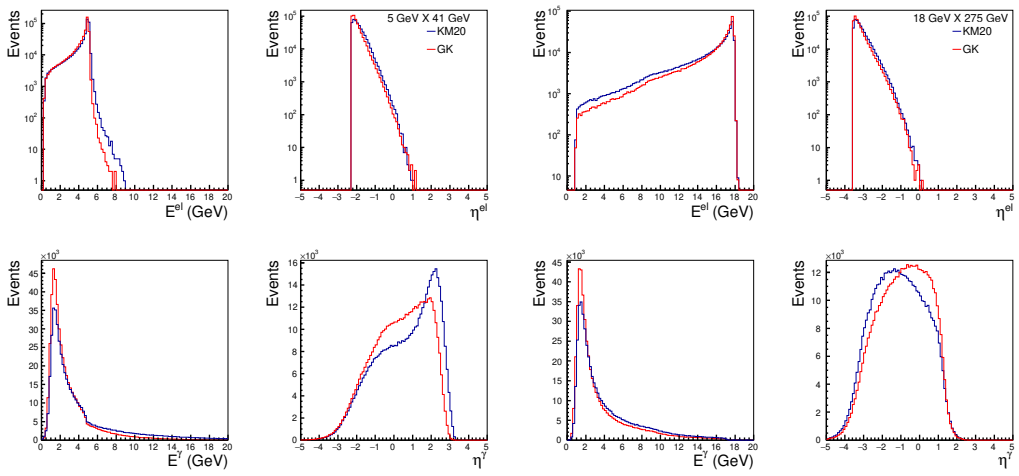

Figure 8.35: Energy and pseudo-rapidity spectra of DVCS events generated according to KM20 (blue) and GK (red) models.

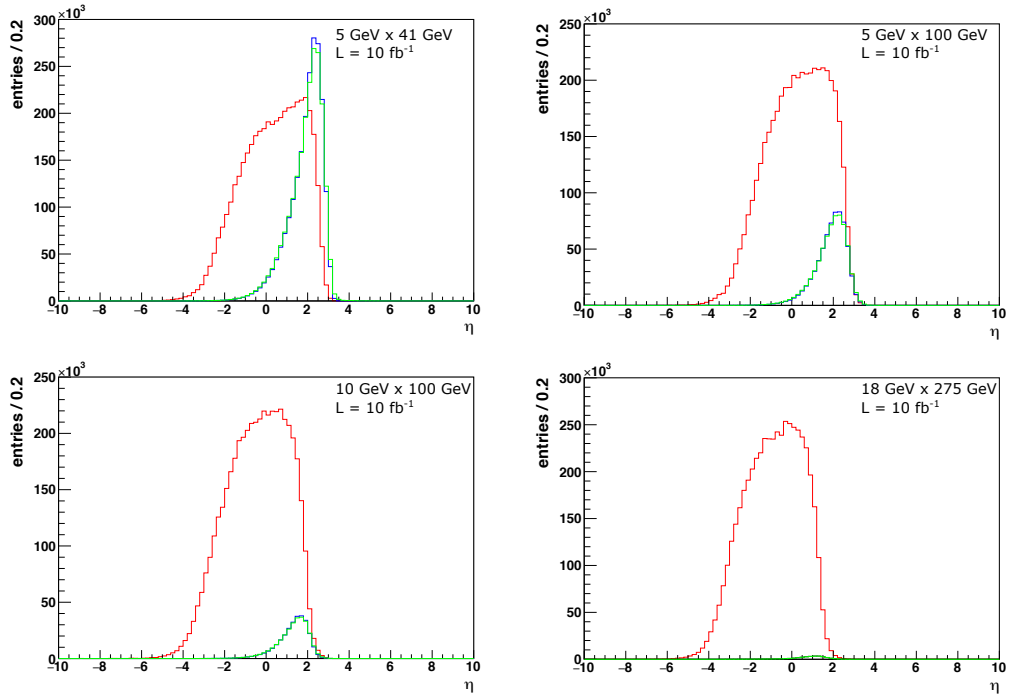

Figure 8.36: Distributions of pseudo-rapidity for DVCS photons (red), exclusive π^0 mesons (blue) and photons coming from decays of $\pi^0 \to \gamma\gamma$ (green, histogram scaled by 12) for four beam energy configurations (see the insert labels) and 10 fb^{-1} of integrated luminosity.

ECALs and cuts on the spacial separation of π^0 decay photons, we may estimate that in

the domain of high-x_{Bj} one may expect a significant yield of DVMP π^0 events with respect to DVCS. The effect of such cuts can be deduced from plots like those show in Fig. 8.38, where spectra of energy and opening angles of photons are shown.

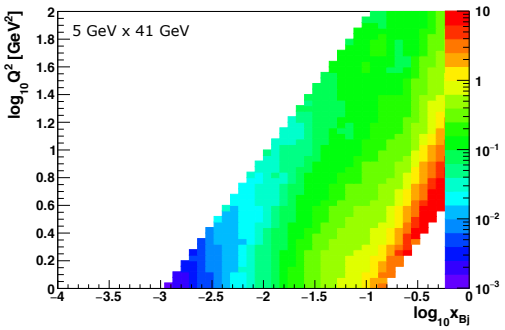

Figure 8.37: Ratio of DVMP π^0 to DVCS event yields in phase-space of (x_{Bj}, Q^2) for 5 GeV $\times$ 41 GeV beam energies. For more details see the text.

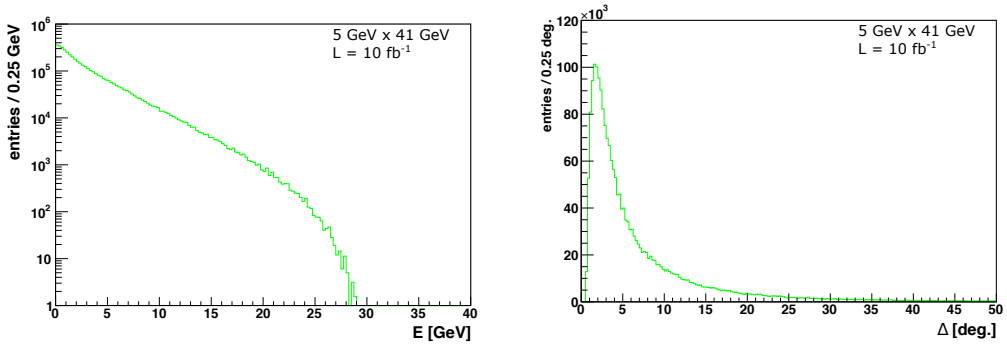

Figure 8.38: energy distribution of photons coming from decays of exclusively produced $\pi^0 \to \gamma\gamma$ (left) and distribution of opening angle between those photons (right). Plots are for 5 GeV $\times$ 41 GeV beam energies and 10 fb^{-1} of integrated luminosity

8.4.2 Timelike Compton Scattering

8.4.3 Neutron target

Neutron GPDs can also be studied at the EIC, where the unique collider experiment at high energy with fully reconstructed final-state particles can provide insights into the neutron substructure. Since there is no easy source of a free neutron target at collider facilities, one of the experimental challenges of constraining the neutron GPDs is to separate the background from nucleus-induced effect when colliding with nuclei. Hereby, the newly